RSC Advances

PAPER

View Article Online
View Journal | View Issue

Cite this: *RSC Adv.*, 2017, **7**, 21713

Interplay between the σ-tetrel bond and σ-halogen bond in $PhSiF_3$···4-iodopyridine···N-base†

Huili Xu, Jianbo Cheng,* Xin Yang, Zhenbo Liu, Xiao Bo and Qingzhong Li*

The ternary complexes of $PhSiF_3$···4-iodopyridine···N-base (N-base = HCN, NH_3, $NHNH_2$, and NH_2CH_3), $PhTF_3$···4-iodopyridine···NH_3 (T = C and Ge), $PhSiY_3$···4-iodopyridine···NH_3 (Y = H and Cl), $PhSiF_3$···4-bromopyridine···NH_3 and the respective binary complexes have been investigated. 4-Halopyridine in these ternary complexes plays a dual role of both a Lewis acid with the σ-hole on the halogen atom in the halogen bond and a Lewis base with the nitrogen atom in the tetrel bond. The interplay between both interactions in the ternary complexes has been analyzed in terms of the binding distance, binding energy, charge transfer, electron density and electrostatic potentials. A synergistic effect is found for the tetrel and halogen bonds in most of the ternary complexes, while a diminutive effect is present for the hydrogen and halogen bonds in $PhCF_3$···4-iodopyridine···NH_3. The magnitude of cooperative energy depends on the strength of both interactions. Interestingly, $PhSiCl_3$···4-iodopyridine has a stronger tetrel bond than $PhSiH_3$···4-iodopyridine, inconsistent with the size of the σ-hole on the Si atom. In addition, the tetrel bond exhibits a partially covalent interaction nature.

Received 19th February 2017
Accepted 12th April 2017

DOI: 10.1039/c7ra02068f

rsc.li/rsc-advances

1. Introduction

Noncovalent interactions have a special importance in supramolecular chemistry, crystal engineering, and biological systems.[1,2] It is well known that hydrogen bonds are the main driving force in maintaining the stability of complex structures.[3,4] Recently, other interactions such as halogen bonds have been widely recognized because of their similarities in geometries and applications with hydrogen bonds. Halogen bonds also play an important role in controlling molecular recognition in biological systems and determining molecular orientation within crystals.[5–9] The origin of the Lewis acid in halogen bonding is mainly attributed to a region of positive electrostatic potential (σ-hole),[10–15] being the consequence of the diminished electron density on the extension of a covalent bond to the halogen atom. The applications of halogen bonds are dependent on their strength, which becomes stronger in the order F ≪ Cl < Br < I. Thus iodine-containing molecules are often used to form a halogen bond in crystal materials and solution.[16–20] In these investigations, the I···N halogen bond has drawn much attention with experimental[20–22] and theoretical[23–25] methods. For example, tetraiodoethynyl resorcinarene cavitands are formed using halogen bonded supramolecular assemblies with the nitrogen in pyridine.[21] In constructing crystal materials, more than one interaction is present, thus cooperative effect occurs, which is one of important properties of noncovalent interactions. It was demonstrated that halogen bonds exhibit cooperative effects with themselves or other interactions,[26–35] through which the strength of halogen bonds is modulated.

Like the halogen atom in halogen bonding, a group 14 atom also acts as a Lewis acid to interact with a Lewis base and the corresponding interaction has been coined as tetrel bonding recently.[36] Actually, this interaction had been explored[37–39] before this term was proposed in 2013. Now tetrel bonding has been attracting more attention due to its roles in crystal materials[40–42] and chemical reactions.[43–45] However, tetrel bonding attracted less interest than hydrogen and halogen bonds; even so, there are relatively many studies that focus on the cooperativity involving tetrel bonds.[46–61] Esrafili *et al.* performed a comparative investigation on the cooperative effects between tetrel bond and other σ-hole bond interactions in complexes YH_3M···NCX···NH_3 (M = C, Si; Y = F, CN and X = Cl, SH, PH_2).[56] *Ab initio* calculations were performed to study the cooperativity between the π-hole tetrel bond and σ-hole halogen bond in complexes XCN···F_2CO···YCN (X = H, F, Cl, Br; Y = F, Cl, Br).[60] Zeng and co-authors[61] discovered a pseudo π-hole in cyclopropane and its derivatives M_3H_6 (M = C, Si, Ge, Sn, Pb), and found that this π-hole is enlarged due to the coexistence of a π-hole tetrel bond and a σ-hole halogen bond in complexes M_3H_6···$(NCF)_n$ (n = 1, 2, 3). The results showed that the strength of tetrel bond can be affected by the coexistence with another interaction.

In the present paper, we study the complexes $PhSiF_3$···4-iodopyridine···N-base (N-base = HCN, NH_3, $NHNH_2$, and

The Laboratory of Theoretical and Computational Chemistry, School of Chemistry and Chemical Engineering, Yantai University, Yantai 264005, People's Republic of China. E-mail: liqingzhong1990@sina.com; Fax: +86 535 6902063; Tel: +86 535 6902063

† Electronic supplementary information (ESI) available. See DOI: 10.1039/c7ra02068f

NH_2CH_3) to investigate the synergistic effect between σ-hole tetrel bond and σ-hole halogen bond and to compare the effect of different N-bases on this synergistic effect. 4-Iodopyridine is a drug intermediate and it is denoted as PyI in the following sections for simplicity. Phenyltrifluorosilane ($PhSiF_3$) turned out to be an original and effective reagent and synthon in organoelemental and organic synthesis.[62] Comparison is made for the complexes of $PhCF_3\cdots PyI\cdots NH_3$, $PhGeF_3\cdots PyI\cdots NH_3$, $PhSiH_3\cdots PyI\cdots NH_3$, $PhSiCl_3\cdots PyI\cdots NH_3$, and $PhSiF_3\cdots PyBr\cdots NH_3$. The synergistic effect between both interactions is characterized in views of binding distances, interaction energies, cooperative energy, and electron density. Natural bond orbital (NBO) and molecular electrostatic potential (MEP) analyses are used to unveil the mechanism of such cooperativity.

2. Computational methods

The geometries of the complexes and monomers were optimized at the RI-MP2/aug-cc-pVTZ[63] level of theory using the TURBOMOLE 6.5 software.[64] For iodine, the aug-cc-pVTZ-PP[65] basis set with pseudopotentials was used to accelerate the calculations and account for relativistic effects. It has been demonstrated that the RI-MP2 method is very convenient for studying a variety of noncovalent interactions in large systems.[66,67] Frequency calculations were also performed at the same level to affirm that the corresponding structures are minima on the potential energy surfaces. The binding energies were calculated with supermolecular method and corrected for the basis set superposition error (BSSE) using the Boys–Bernardi counterpoise technique.[68]

MEPs were computed on the 0.001 au contour of electronic density at the MP2/aug-cc-pVTZ level using the Wave Function Analysis-Surface Analysis Suite (WFA-SAS) program.[69] The topological analysis of the electron density at bond critical point (BCP) was performed by means of the AIM2000 program.[70] NBO analysis[71] was carried out at the HF/aug-cc-pVTZ level using NBO 5.0 program.[72] Non-covalent interaction (NCI) index[73] was plotted with the Multiwfn program.[74]

3. Results and discussion

3.1 MEPs and geometries

Fig. 1 shows the MEP maps of $PhSiF_3$ and 4-iodopyridine (PyI). Four σ-holes (red region) are found on the tetrahedral surfaces of the Si atom in $PhSiF_3$, locating along the C–Si and F–Si bond ends, respectively. We pay our attention to the σ-hole at the C–Si end, having a positive MEP of 134.98 kJ mol^{-1} (Table 1). This value amounts to 15.85 and 138.43 kJ mol^{-1} in $PhCF_3$ and $PhGeF_3$, respectively. Clearly, the σ-hole at the C–T end enlarges in the sequence C ≪ Si < Ge, due to the smaller electronegativity and larger polarizability of the heavier T atom. When $-SiF_3$ is respectively replaced by $-SiH_3$ and $-SiCl_3$, the corresponding value is 82.59 and 55.84 kJ mol^{-1}, which is smaller than that in $PhSiF_3$ owing to the smaller electronegativity of H and Cl atoms. Interestingly, the σ-hole at the C–Si end in $PhSiCl_3$ has a smaller MEP than that in $PhSiH_3$, which is inconsistent with the relative electronegativity of both H and Cl elements. We ascribe it to a strong orbital interaction from the lone pair on the Cl atom to the C–Si* anti-bonding orbital in $PhSiCl_3$ (Fig. S1†). There are three Lp(Cl) → σ*(C–Si) orbital interactions in $PhSiCl_3$ and the sum of their perturbation energies is ~116 kJ mol^{-1}. Similarly, a σ-hole is found at the outer of C–I bond in PyI and it has a greater MEP than that in PyBr. On the other hand, the N atom of PyI is surrounded by a negative MEP, and its value is almost equal to that in PyBr. That is, the halogen substituent in pyridine has a slight effect on the basicity of its N atom. Therefore, the N atom of PyX (X = Br and I) acts as a Lewis base to form a tetrel bond with the tetrel atom of $PhTF_3$ (T = C, Si, Ge) and the X atom acts as a Lewis acid to form a halogen bond with the N-base. The structures of the corresponding complexes are shown in Fig. 2.

Table 2 presents the binding distances in the dyads and triads. One can see that the binding distances of both tetrel and halogen bonds are shorter in the trials except $PhCF_3\cdots PyI\cdots NH_3$ when the complex varies from the dyad to the triad. In $PhCF_3\cdots PyI\cdots NH_3$, the two interatomic separations are longer in the triad with respect to those in the dyad. Moreover, the shortening of the halogen bonding distance is much larger than that of tetrel bonding distance in most triads. For the tetrel bond, the longer the binding distance in the dyad, the greater the shortening of the binding distance in the triad. This is also hold true for the binding distance of halogen bond in the complexes of $PhSiF_3\cdots PyI\cdots$N-base. The shortening of halogen bonding distance in $PyI\cdots NH_3$ is larger for the shorter tetrel bonding distance. The largest shortening of halogen bonding distance is 0.684 Å in $PhGeF_3\cdots PyI\cdots NH_3$ and $PhSiCl_3\cdots PyI\cdots NH_3$.

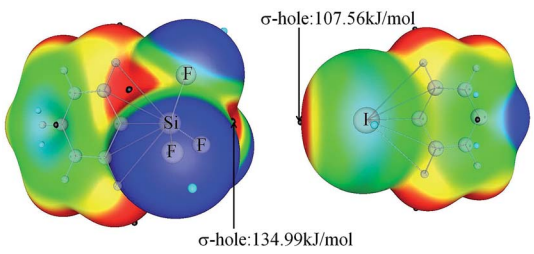

Fig. 1 MEP maps of $PhSiF_3$ (left) and 4-iodopyridine (right). Color ranges in kJ mol^{-1}, are: red, greater than 47; yellow, between 47 and 13; green, between 13 and −26, blue, less than −26.

Table 1 The most positive electrostatic potentials (V_{max}, kJ mol^{-1}) on the T and X atoms and the most negative electrostatic potential (V_{min}, kJ mol^{-1}) on the N atom of PyX (X = Br and I)[a]

Molecules	$V_{max,T}$	Complexes	$V_{max,X}$	Complexes	$V_{min,N}$
$PhCF_3$	15.85	$PhCF_3\cdots PyI$	96.43	$PyI\cdots NH_3$	−161.80
$PhSiF_3$	134.98	$PhSiF_3\cdots PyI$	145.39	$PyI\cdots NCH$	−161.89
$PhGeF_3$	138.43	$PhGeF_3\cdots PyI$	150.69	$PyI\cdots NHCH_2$	−161.86
$PhSiH_3$	82.59	$PhSiH_3\cdots PyI$	119.52	$PyI\cdots NH_2CH_3$	−162.86
$PhSiCl_3$	55.84	$PhSiCl_3\cdots PyI$	150.15	$PyBr\cdots NH_3$	−157.84
—	—	$PhSiF_3\cdots PyBr$	113.01	—	—

[a] Note: $V_{max,X}$ is 75.29 and 107.56 kJ mol^{-1} in PyBr and PyI, respectively. $V_{min,N}$ is −141.67 and −142.02 kJ mol^{-1} in PyBr and PyI, respectively.

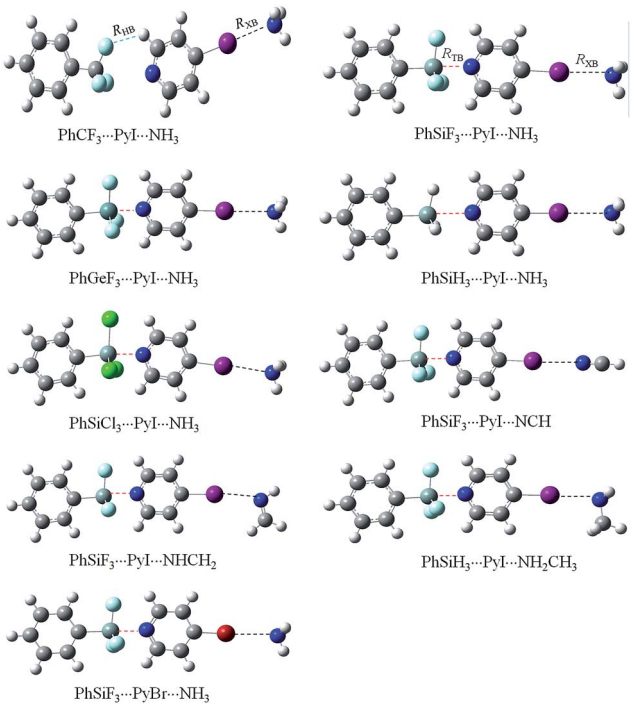

Fig. 2 Optimized structures of the ternary complexes.

3.2 Binding energies

Table 3 presents the total binding energy in the triads as well as the binding energies of tetrel and halogen bonds in the binary and the ternary complexes. The total binding energy is changed in a wide range from 16.95 kJ mol^{-1} in $PhCF_3\cdots PyI\cdots NH_3$ to 148.38 kJ mol^{-1} in $PhGeF_3\cdots PyI\cdots NH_3$. The binding energy of halogen bond is related with the nature of the halogen donor and the N-base. It is expected that PyI forms a stronger halogen bond with NH_3 than PyBr, which is consistent with the magnitude of σ-hole on the halogen atom. The halogen bond is stronger in the order HCN(sp) < $NH_3(sp^3)$ < $NHCH_2(sp^2)$ < $NH_2CH_3(sp^3)$. Obviously, the basicity of N-base is related with the electronegativity of N element. In addition, the methyl group in the electron donor plays an electron-donating role in the formation of halogen bond.[48] The strength of tetrel bond is mainly dependent on the nature of tetrel atom and its substituents, but it shows a slight dependence on the halogen substitution in pyridine. The binding energy of tetrel bond is almost equal in both $PhSiF_3\cdots PyBr$ and $PhSiF_3\cdots PyI$, consistent with the negative MEP on the N atom of PyX (X = Br and I). $PhGeF_3$ forms a stronger tetrel bond than $PhSiF_3$ and their binding energies have a difference of about 25 kJ mol^{-1}. However, the positive MEP on the Ge atom in $PhGeF_3$ is larger only by 3.45 kJ mol^{-1} than that on the Si atom in $PhSiF_3$. This indicates that not only electrostatic interaction but also polarization interaction is responsible for the stability of tetrel bonded complexes. The binding energy of tetrel bond is more negative in $PhSiF_3\cdots PyI$ than that in $PhSiH_3\cdots PyI$, having a consistent change with the positive MEP on the Si atom in both molecules. $PhSiCl_3$ forms a weaker tetrel bond with PyI than $PhSiF_3$ but a stronger tetrel bond than $PhSiH_3$. The former is consistent with the change of σ-hole on the Si atom, but the latter is reverse to the change of σ-hole on the Si atom. This inconsistency is also attributed to the larger polarization in $PhSiCl_3\cdots PyI$ than in $PhSiH_3\cdots PyI$. The larger polarization in $PhSiCl_3\cdots PyI$ can be visualized by comparing the electron density shift on the silicon atom in $PhSiCl_3\cdots PyI$ and $PhSiH_3\cdots PyI$. As shown in Fig. 3, the red area on the silicon atom in $PhSiCl_3\cdots PyI$ is larger than that in $PhSiH_3\cdots PyI$. This indicates that the silicon atom in $PhSiCl_3\cdots PyI$ suffers larger polarization in the formation of tetrel bond. Similarly, the role of polarization in halogen bonds has been unveiled in $CF_3Cl\cdots OH_2$ complex by Clark *et al.*[75] Halogen bond is weaker than tetrel bond in most dyads but is stronger than hydrogen bond in $PhCF_3\cdots PyI$. The binding energy of tetrel bond is larger than 90 kJ mol^{-1} in $PhTY_3\cdots PyX$ (T = Si and Ge; Y = F and Cl; X = Br and I). Thus this tetrel bond is very strong, resulting in a prominent deformation of $-TY_3$ group. This deformation has been considered in calculating the binding energy of tetrel bond by using the energy of the monomer in the complexes. The magnitude of $-TY_3$ deformation can be estimated with the change of angle C–T–Y in the complex relative to the monomer (Table S1†). This angle is larger than 10° in $PhTY_3\cdots PyX$ (T = Si and Ge; Y = F and Cl; X = Br and I). Thus the deformation energy has the larger contribution to the strong tetrel bond in the above complexes. The prominent deformation of $-TY_3$ group is mainly caused by the formation of a partially covalent tetrel bond.

Table 2 Intermolecular distances (*R*, Å) in the triads and their changes (Δ*R*, Å) relative to the corresponding dyads[a]

Triads	$R_{TB/HB}$	$\Delta R_{TB/HB}$	R_{XB}	ΔR_{XB}
$PhCF_3\cdots PyI\cdots NH_3$	2.4271(2.4181)	0.0096	3.0506(3.0463)	0.0043
$PhSiF_3\cdots PyI\cdots NH_3$	2.0980(2.1278)	−0.0298	2.9852	−0.0611
$PhGeF_3\cdots PyI\cdots NH_3$	2.0642(2.0787)	−0.0145	2.9779	−0.0684
$PhSiH_3\cdots PyI\cdots NH_3$	2.5442(2.6189)	−0.0747	3.0157	−0.0306
$PhSiCl_3\cdots PyI\cdots NH_3$	2.1058(2.1413)	−0.0355	2.9779	−0.0684
$PhSiF_3\cdots PyI\cdots NCH$	2.1013	−0.0265	3.0587(3.1142)	−0.0555
$PhSiF_3\cdots PyI\cdots NHCH_2$	2.0981	−0.0297	2.9151(2.9749)	−0.0598
$PhSiF_3\cdots PyI\cdots NH_2CH_3$	2.0958	−0.0320	2.8804(2.9381)	−0.0577
$PhSiF_3\cdots PyBr\cdots NH_3$	2.1011(2.1271)	−0.0260	3.0174(3.0589)	−0.0415

[a] Note: data in parentheses are from the respective dyads.

Table 3 Total interaction energy (ΔE_{total}), interaction energies of tetrel bond (ΔE_{TB}) and halogen bond (ΔE_{XB}), and cooperative energy (E_{coop}) in the triads. All are in kJ mol^{-1}[a]

Triads	ΔE_{total}	$\Delta E_{TB/HB}$	ΔE_{XB}	E_{coop}
$PhCF_3\cdots PyI\cdots NH_3$	−16.95	−1.42(−2.42)	−14.54(−15.48)	0.68(4.0%)
$PhSiF_3\cdots PyI\cdots NH_3$	−126.27	−111.20(−96.94)	−20.25	−13.51(10.7%)
$PhGeF_3\cdots PyI\cdots NH_3$	−148.38	−133.42(−121.84)	−20.79	−10.81(7.3%)
$PhSiH_3\cdots PyI\cdots NH_3$	−34.95	−19.72(−16.39)	−17.29	−3.03(8.7%)
$PhSiCl_3\cdots PyI\cdots NH_3$	−122.27	−107.21(−92.85)	−20.92	−13.81(11.3%)
$PhSiF_3\cdots PyI\cdots NCH$	−119.94	−109.42	−14.96(−10.92)	−2.72(2.3%)
$PhSiF_3\cdots PyI\cdots NHCH_2$	−128.22	−111.23	−22.18(−17.29)	−13.64(10.6%)
$PhSiF_3\cdots PyI\cdots NH_2CH_3$	−132.04	−112.53	−25.25(−19.95)	−14.85(11.2%)
$PhSiF_3\cdots PyBr\cdots NH_3$	−118.11	−108.85(−96.90)	−13.49(−9.43)	−11.42(9.7%)

[a] Note: data in parentheses are from the respective dyads. The interaction energies of tetrel and halogen bonds in the triad are calculated with formula of $\Delta E_{A\text{–}BC} = E_{A\text{–}BC(T)} - E_{A(T)} - E_{BC(T)}$, where $E_{A\text{–}BC(T)}$ is the energy of A–BC corrected for BSSE with counterpoise = 2, $E_{A(T)}$ the energy of A in the triad, and $E_{BC(T)}$ the energy of BC in the triad.

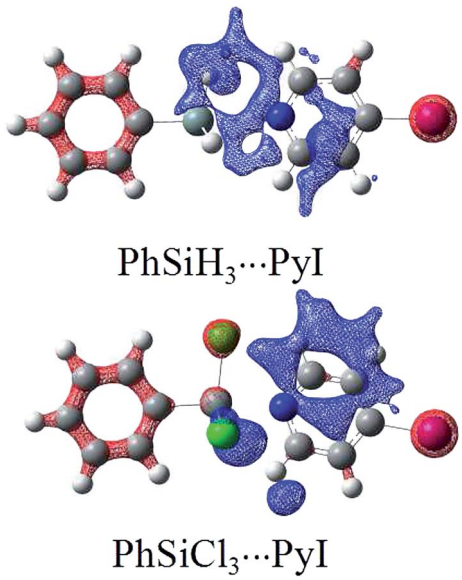

Fig. 3 Electron density shifts in $PhSiH_3\cdots PyI$ and $PhSiCl_3\cdots PyI$. Contours are shown at the 0.25 au level. Red/blue regions indicate increased/decreased density.

In most triads, the binding energies of tetrel and halogen bonds are more negative than those in the dyads, indicating that both tetrel and halogen bonds are stronger in the triads. Thus there exists positive cooperativity between tetrel and halogen bonds in the triads except $PhCF_3\cdots PyI\cdots NH_3$. However, the binding energies of both interactions in $PhCF_3\cdots PyI\cdots NH_3$ are less negative, showing that they are weaker in this triad. As a result, negative cooperativity is found between hydrogen and halogen bonds in $PhCF_3\cdots PyI\cdots NH_3$. Table S2† lists the increased/decreased percentage of binding energies of both interactions in the triads relative to those in the dyads. It is found that this percentage is pertinent to the relative strength of both interactions. Clearly, the weaker interaction has a larger increased/decreased percentage than the stronger one. Specially, the hydrogen bond has a larger weakening than the halogen bond in $PhCF_3\cdots PyI\cdots NH_3$; the tetrel bond has a larger enhancement than the halogen bond in $PhSiH_3\cdots PyI\cdots NH_3$, while the halogen bond has a larger enhancement than the tetrel bond in other triads.

According to the electrostatic nature of tetrel and halogen bonds, the change of binding energy in the triads can be understood with the change of the negative MEP on the N atom of PyX in PyX···N-base and the positive MEP on the X atom of PyX in $PhTY_3\cdots PyX$ (Table 1). The former is more negative in PyX···N-base and the latter is more positive in $PhTY_3\cdots PyX$ (T = Si and Ge). This indicates that the N atom of PyX in PyX···N-base is a stronger Lewis base and the X atom of PyX in $PhTY_3\cdots PyX$ (T = Si and Ge) is a stronger Lewis acid. Consequently, the former forms a stronger tetrel bond and the latter forms a stronger halogen bond. However, the positive MEP on the iodine atom of PyI is smaller in $PhCF_3\cdots PyI$, thus it is a weaker Lewis acid and forms a weaker halogen bond in $PhCF_3\cdots PyI\cdots NH_3$. The positive MEP on the H atom adjoined to the N atom of pyridine reduces from 86.90 kJ mol^{-1} in 4-iodopyridine to 66.36 kJ mol^{-1} in $PyI\cdots NH_3$, thus a weaker hydrogen bond is obtained in $PhCF_3\cdots PyI\cdots NH_3$.

This cooperative effect can also be better estimated with cooperative energy (E_{coop}), calculated with the formulas of $E_{coop} = \Delta E_{total} - \Delta E_{TB(D)} - \Delta E_{XB(D)}$, where ΔE_{total} is the total binding energy of triad, $\Delta E_{TB(D)}$ and $\Delta E_{XB(D)}$ are the binding energies of tetrel bond and halogen bond in the optimized dyads, respectively. It is found from Table 3 that this term is negative in most triads but positive in $PhCF_3\cdots PyI\cdots NH_3$, confirming the positive cooperativity in the former and the negative one in the latter. The cooperative energy amounts to about 2.3–11.3% of the total binding energy. The smallest percentage is found in $PhSiF_3\cdots PyI\cdots NCH$ and the largest percentage is found in $PhSiCl_3\cdots PyI\cdots NH_3$ and $PhSiF_3\cdots PyI\cdots NH_2CH_3$. The contribution of cooperative energy to the total binding energy is small if one of two interactions is weak. This percentage in most triads is larger than that reported in hydrogen bonds (less than 6%).[76]

3.3 AIM analyses

Fig. 4 shows the molecular maps of the dyads. A H···F BCP and two N···F BCPs are found in $PhCF_3\cdots PyI$, and the former confirms the existence of C–H···F hydrogen bond. The tetrel bond in $PhTY_3\cdots PyX$ (T = Si and Ge) is characterized with

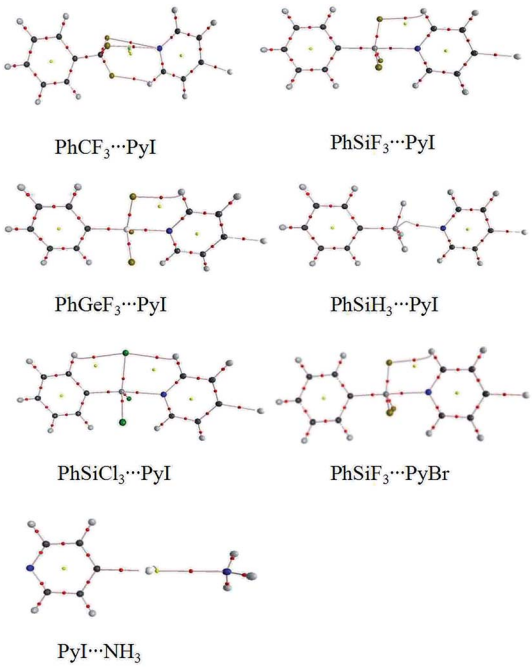

Fig. 4 Molecular graph of the binary complexes.

a T···N BCP. In addition, a H···F/Cl BCP is also found in the strong tetrel bonded complexes. This H···F/Cl BCP corresponds to a C–H···F/Cl hydrogen bond. However, such BCP is not present in $PhSiH_3$···PyI. Thus the C–H···Cl hydrogen bond has some contribution to the larger binding energy in $PhSiCl_3$···PyI relative to that in $PhSiH_3$···PyI. A X···N BCP is found in the halogen bonded complexes.

The electron density, Laplacian, and energy density at these BCPs are collected in Table 4. The electron density at the X···N BCP is smaller than 0.024 au and that at the Si/Ge···N BCP is larger than 0.021 au. The electron density at the H···F BCP is very small, consistent with the weak C–H···F interaction. The Laplacian at the T···N BCP is a large positive value in $PhTY_3$···PyX (T = Si and Ge) and its energy density is negative. This shows that the tetrel bond is a partially covalent interaction with a big strength.[77] The positive energy density at the X···N BCP supports the conclusion that halogen bond is electrostatic in nature. The electron density at the X···N BCP is increased in the sequence HCN < NH_3 < $NHCH_2$< NH_2CH_3, showing that the electron density can be used to measure the strength of halogen bond. This conclusion holds true for the tetrel bond. In Fig. 5, we plotted the relationship between the electron density at the same BCP and the corresponding atom separation for the tetrel and halogen bonds. An exponential relationship is found for the Si···N tetrel bond but a linear relationship for the I···N halogen bond. Table S3† presents the change of electron density ($\Delta\rho$) at the triads relative to the dyads. The value of $\Delta\rho$ is positive in most triads with an exception of $PhCF_3$···PyI···NH_3. The increase/decrease of electron density confirms the change of both interactions in the triads.

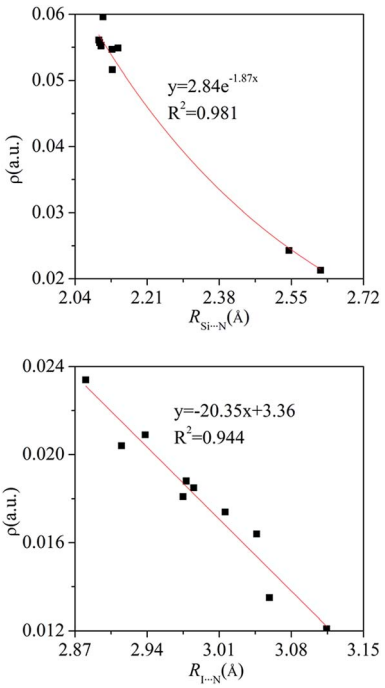

Fig. 5 Electron density (ρ) at the same BCP *versus* the corresponding atom separation (R) for the Si···N tetrel bond and I···N halogen bond in the binary and ternary complexes.

Table 4 Electron density (ρ, au), Laplacian ($\nabla^2\rho$, au), and energy density (H, au) at the intermolecular bond critical points in the triads[a]

Triads	ρ_{TB}	$\nabla^2\rho_{TB}$	H_{TB}	ρ_{XB}	$\nabla^2\rho_{XB}$	H_{XB}
$PhCF_3$···PyI···NH_3	0.0073	0.0355	0.0019	0.0163	0.0544	0.0016
$PhSiF_3$···PyI···NH_3	0.0557	0.2167	−0.0169	0.0185	0.0605	0.0014
$PhGeF_3$···PyI···NH_3	0.0844	0.2419	−0.0342	0.0188	0.0612	0.0014
$PhSiH_3$···PyI···NH_3	0.0243	0.0565	−0.0024	0.0174	0.0577	0.0015
$PhSiCl_3$···PyI···NH_3	0.0596	0.1863	−0.0211	0.0188	0.0612	0.0014
$PhSiF_3$···PyI···NCH	0.0553	0.2141	−0.0167	0.0135	0.0541	0.0022
$PhSiF_3$···PyI···$NHCH_2$	0.0557	0.2163	−0.0169	0.0204	0.0687	0.0013
$PhSiF_3$···PyI···NH_2CH_3	0.0561	0.2180	−0.0171	0.0234	0.0717	0.0006
$PhSiF_3$···PyBr···NH_3	0.0552	0.2144	−0.0167	0.0139	0.0518	0.0020

[a] Note: The corresponding values are from the H···F BCP in $PhCF_3$···PyI···NH_3. The corresponding values at the N···F BCP are 0.0039, 0.0159 and 0.0008 au in $PhCF_3$···PyI···NH_3.

The cooperativity between both interactions in the ternary complexes can be visualized by the NCI analysis. The ternary complexes of $PhCF_3\cdots PyI\cdots NH_3$ and $PhSiF_3\cdots PyI\cdots NH_3$ are respectively chosen as an example to obtain visualization of the negative and positive cooperativity. Fig. 6 shows the plot of the reduced density gradient *versus* sign(λ_2)ρ in these complexes. The F···H hydrogen bond in $PhCF_3\cdots PyI$ and I···N halogen bond in $PyI\cdots NH_3$ are characterized by the pink and green spikes, respectively. Although their shifts are not obviously observed in $PhCF_3\cdots PyI\cdots NH_3$, a tiny shift to the lower electron density can be found by a careful comparison, confirming the negative cooperativity in $PhCF_3\cdots PyI\cdots NH_3$. The tetrel bond in $PhSiF_3\cdots PyI$ and halogen bond in $PyI\cdots NH_3$ are also represented by the pink and green spikes. In $PhSiF_3\cdots PyI\cdots NH_3$, the corresponding spikes move to the higher electron density, thus the positive cooperativity is present in this ternary complex.

3.4 NBO analyses

The interactions in these complexes were analyzed in views of orbital interactions and charge transfer. There are two orbital interactions of Lp(N) → p^*_T and Lp(N) → σ^*_{C-T} in the tetrel bonded complexes of $PhTF_3\cdots PyX$ (T = Si and Ge), where Lp(N) denotes the lone pair orbital on N atom, p^*_T the empty p orbital on T atom, and σ^*_{C-T} the C–T antibonding orbital. Lp(N) → σ^*_{C-T} is still present in $PhSiY_3\cdots PyI$ (Y = H and Cl), but Lp(N) → p^*_T is replaced by Lp(N) → $\sigma^*_{Si-H(Cl)}$. Only Lp(F) → σ^*_{C-H}/Lp(N) → σ^*_{C-X} is found in the hydrogen/halogen bond. These orbital interactions are estimated with second-order perturbation energies (Table 5). In $PhTF_3\cdots PyX$ (T = Si and Ge), Lp(N) → p^*_T is far stronger than Lp(N) → σ^*_{C-T}, which is a feature of strong tetrel bonds. For the weak tetrel bond of $PhSiH_3\cdots PyI$, Lp(N) → p^*_{Si} is not present and Lp(N) → σ^*_{C-Si} is stronger than Lp(N) → σ^*_{Si-H}, where the sum of perturbation energy of three Lp(N) → σ^*_{Si-H} is listed in Table 5. In $PhSiCl_3\cdots PyI$, Lp(N) → p^*_{Si} is also not present, but Lp(N) → σ^*_{C-Si} is weaker than Lp(N) → σ^*_{Si-Cl}. The three strong Lp(N) → σ^*_{Si-Cl} orbital interactions are partly responsible for the strong tetrel bond in $PhSiCl_3\cdots PyI$. Lp(F) → σ^*_{C-H} is very weak in $PhCF_3\cdots PyI$, corresponding to the weak C–H···F hydrogen bond. Lp(N) → σ^*_{C-X} has an inconsistent change with the interaction energy of halogen bond, indicating the less importance of orbital interaction in the formation of halogen bond. The changes of second-order perturbation energies in the triads relative to the dyads are given in Table S4.† The second-order perturbation energies of the above orbital interactions are increased in most triads except $PhCF_3\cdots PyI\cdots NH_3$, where they are almost not changed. The strengthening of Lp(N) → p^*_T/Lp(N) → $\sigma^*_{Si-H(Cl)}$ is larger than that of Lp(N) → σ^*_{C-T} and Lp(N) → σ^*_{C-X} in $PhTF_3\cdots PyX\cdots$N-base/$PhSiY_3\cdots PyI\cdots NH_3$ (Y = H and Cl). That is, the orbital interaction has some contribution to the cooperativity between tetrel and halogen bonds. However, the orbital interaction has a slight contribution to the interplay between hydrogen and halogen bonds in $PhCF_3\cdots PyI\cdots NH_3$.

Table 5 Second-order perturbation energies ($E^{(2)}$, kJ mol^{-1}) of Lp(N) → $p^*_T(1)$/Lp(N) → $\sigma^*_{C-T}(2)$ in the tetrel bond and Lp(N) → $\sigma^*_{C-X}(3)$ in the halogen bond in the triads[a]

Triads	$E^{(2)}_1$	$E^{(2)}_2$	$E^{(2)}_3$
$PhCF_3\cdots PyI\cdots NH_3$	0.92(0.92)	—	29.18(29.59)
$PhSiF_3\cdots PyI\cdots NH_3$	617.89(599.99)	17.60(16.18)	36.53
$PhGeF_3\cdots PyI\cdots NH_3$	803.06(762.93)	8.53(8.36)	37.41
$PhSiH_3\cdots PyI\cdots NH_3$	54.01(41.26)	46.06(38.62)	32.85
$PhSiCl_3\cdots PyI\cdots NH_3$	331.85(304.97)	83.52(80.51)	37.62
$PhSiF_3\cdots PyI\cdots NCH$	613.08(561.96)	17.26(16.18)	17.43(14.04)
$PhSiF_3\cdots PyI\cdots NHCH_2$	619.94(599.99)	17.39(16.18)	34.53(26.79)
$PhSiF_3\cdots PyI\cdots NH_2CH_3$	624.58(561.96)	17.47(16.18)	45.19(36.16)
$PhSiF_3\cdots PyBr\cdots NH_3$	612.12(560.75)	17.31(16.30)	17.97(15.30)

[a] Note: $E^{(2)}_1$ corresponds to Lp(F) → σ^*_{C-H} in $PhCF_3\cdots PyI\cdots NH_3$ and Lp(N) → $\sigma^*_{Si-H/Cl}$ in $PhSiH_3\cdots PyI\cdots NH_3$/$PhSiCl_3\cdots PyI\cdots NH_3$, respectively. Data in parentheses are from the respective dyads.

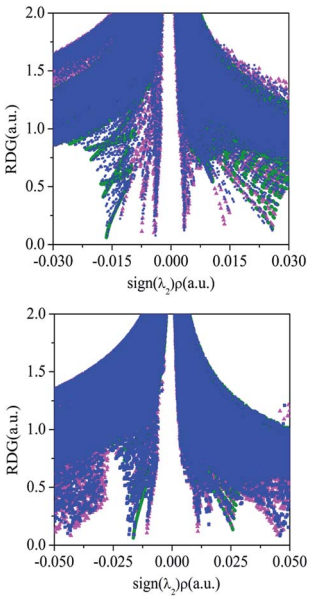

Fig. 6 Reduced density gradient (RDG) *versus* sign(λ_2)ρ in the ternary complexes (blue) of $PhCF_3\cdots PyI\cdots NH_3$ (up) and $PhSiF_3\cdots PyI\cdots NH_3$ (down) as well as the corresponding hydrogen/tetrel (pink) and halogen (green) bonded binary complexes.

Table 6 presents the charge transfer (CT) in the ternary complexes and its change (ΔCT) relative to the corresponding binary complexes. One can see that CT is much larger in the tetrel bond than that in the halogen bond but it is much smaller in the hydrogen bond than that in the halogen bond. Generally, the bigger CT corresponds to a stronger interaction although there is not a good relationship between CT and binding energy. There are some exceptions. For example, CT is larger in $PhSiCl_3\cdots PyI$ than that in $PhSiF_3\cdots PyI$, which disagrees with the change of binding energy. The larger CT in $PhSiCl_3\cdots PyI$ is partly attributed to the greater polarization of Cl atom. ΔCT is positive for the tetrel and halogen bonds but negative for the hydrogen and halogen bonds in the triads, indicating that charge transfer is also important in strengthening both interactions.

Table 6 Charge transfer (CT, e) of both interactions in the triads and its change (ΔCT, e) in the triad relative to the corresponding dyad[a]

Triads	$CT_{TB/HB}$	CT_{XB}	$\Delta CT_{TB/HB}$	ΔCT_{XB}
$PhCF_3\cdots PyI\cdots NH_3$	0.0015(0.0019)	0.0182(0.0186)	−0.0004	−0.0004
$PhSiF_3\cdots PyI\cdots NH_3$	0.1358(0.1243)	0.0234(0.0186)	0.0115	0.0048
$PhGeF_3\cdots PyI\cdots NH_3$	0.1737(0.1647)	0.0241(0.0186)	0.0090	0.0055
$PhSiH_3\cdots PyI\cdots NH_3$	0.0443(0.0349)	0.0207(0.0186)	0.0094	0.0021
$PhSiCl_3\cdots PyI\cdots NH_3$	0.1511(0.1372)	0.0241(0.0186)	0.0139	0.0055
$PhSiF_3\cdots PyI\cdots NCH$	0.1350(0.1234)	0.0061(0.0044)	0.0107	0.0017
$PhSiF_3\cdots PyI\cdots NHCH_2$	0.1366(0.1234)	0.0195(0.0145)	0.0123	0.0050
$PhSiF_3\cdots PyI\cdots NH_2CH_3$	0.1375(0.1234)	0.0297(0.0234)	0.0132	0.0063
$PhSiF_3\cdots PyBr\cdots NH_3$	0.1348(0.1245)	0.0108(0.0089)	0.0103	0.0019

[a] Note: data in parentheses are CT in the respective dyads.

4. Conclusions

Ab initio calculations have been performed to study the σ-tetrel bond and σ-halogen bond in the ternary complexes. $PhTF_3$ (T = Si and Ge) forms a stronger tetrel bond with 4-iodopyridine, while $PhCF_3$ forms a weaker hydrogen bond with 4-iodopyridine. 4-Iodopyridine forms a halogen bond with a series of nitrogen bases. The Si atom of $PhSiCl_3$ has the small σ-hole than that of $PhSiH_3$, but the former forms a stronger tetrel bond than the latter. The tetrel bond exhibits a nature of partially covalent interaction although it is dominated by electrostatic interaction. In most ternary complexes, both tetrel and halogen bonds are strengthened with positive cooperativity. However, both hydrogen and halogen bonds in $PhCF_3\cdots$4-iodopyridine$\cdots NH_3$ are weakened with negative cooperativity. The cooperativity between tetrel and halogen bonds is attributed to the electrostatic and orbital interactions. The cooperative energy grows up in the order HCN < NH_3 < $NHCH_2$ < NH_2CH_3, depending on the strength of halogen bond. The title complexes are involved with molecules usually used in crystal materials, thus these results are significant for the applications of tetrel and halogen bonds in these fields.

Acknowledgements

This work was supported by the National Natural Science Foundation of China (21573188).

References

1 B. Rybtchinski, *ACS Nano*, 2011, **5**, 6791–6818.
2 K. Müller-Dethlefs and P. Hobza, *Chem. Rev.*, 2000, **100**, 143–168.
3 Q. Shao and Y. Q. Gao, *J. Chem. Theory Comput.*, 2010, **6**, 3750–3760.
4 A. J. Parker, J. Stewart, K. J. Donald and C. A. Parish, *J. Am. Chem. Soc.*, 2012, **134**, 5165–5172.
5 P. Auffinger, F. A. Hays, E. Westhof and P. S. Ho, *Proc. Natl. Acad. Sci. U. S. A.*, 2004, **101**, 16789–16794.
6 S. Triguero, R. Llusar, V. Polo and M. Fourmigúe, *Cryst. Growth Des.*, 2008, **8**, 2241–2247.
7 P. Metrangolo, Y. Carcenac, M. Lahtinen, T. Pilati, K. Rissanen, A. Vij and G. Resnati, *Science*, 2009, **323**, 1461–1464.
8 K. Ueda, M. Oguni and T. Asaji, *Cryst. Growth Des.*, 2014, **14**, 6189–6196.
9 S. W. Robinson, C. L. Mustoe, N. G. White, A. Brown, A. L. Thompson, P. Kennepohl and P. D. Beer, *J. Am. Chem. Soc.*, 2015, **137**, 499–507.
10 P. Politzer, P. Lane, M. C. Concha, Y. G. Ma and J. S. Murray, *J. Mol. Model.*, 2007, **13**, 305–311.
11 P. Politzer, J. S. Murray and M. C. Concha, *J. Mol. Model.*, 2008, **14**, 659–665.
12 K. E. Riley, J. S. Murray, P. Politzer, M. C. Concha and P. Hobza, *J. Chem. Theory Comput.*, 2009, **5**, 155–163.
13 K. E. Riley, J. S. Murray, J. Fanfrlík, J. Řezáč, R. J. Solá, M. C. Concha, F. M. Ramos and P. Politzer, *J. Mol. Model.*, 2011, **17**, 3309–3318.
14 J. S. Murray, P. Lane, T. Clark, K. E. Riley and P. Politzer, *J. Mol. Model.*, 2012, **18**, 541–548.
15 P. Politzer and J. S. Murray, *Theor. Chem. Acc.*, 2012, **131**, 1114.
16 A. C. C. Carlsson, J. Gräfenstein, A. Budnjo, J. L. Laurila, J. Bergquist, A. Karim, R. Kleinmaier, U. Brath and M. Erdélyi, *J. Am. Chem. Soc.*, 2012, **134**, 5706–5715.
17 Q. N. Zheng, X. H. Liu, T. Chen, H. J. Yan, T. Cook, D. Wang, P. J. Stang and L. J. Wan, *J. Am. Chem. Soc.*, 2015, **137**, 6128–6131.
18 E. Cariati, G. Cavallo, A. Forni, G. Leem, P. Metrangolo, F. Meyer, T. Pilati, G. Resnati, S. Righetto, G. Terraneo and E. Tordin, *Cryst. Growth Des.*, 2011, **11**, 5642–5648.
19 F. C. Pigge, P. P. Kapadia and D. C. Swenson, *CrystEngComm*, 2013, **15**, 4386–4391.
20 L. C. Roper, C. Präsang, V. N. Kozhevnikov, A. C. Whitwood, P. B. Karadakov and D. W. Bruce, *Cryst. Growth Des.*, 2010, **10**, 3710–3720.
21 L. Turunen, N. K. Beyeh, F. Pan, A. Valkonen and K. Rissanen, *Chem. Commun.*, 2014, **50**, 15920–15923.
22 E. M. Karlsen and J. Spanget-Larsen, *Chem. Phys. Lett.*, 2009, **473**, 227–232.
23 A. Bauzá, D. Quiñonero, A. Frontera and P. M. Deyà, *Phys. Chem. Chem. Phys.*, 2011, **13**, 20371–20379.
24 S. Tsuzuki, A. Wakisaka, T. Ono and T. Sonoda, *Chem.–Eur. J.*, 2012, **18**, 951–960.

25 A. C. C. Carlsson, M. Uhrbom, A. Karim, U. Brath, J. Gräfenstein and M. Erdélyi, *CrystEngComm*, 2013, **15**, 3087–3092.
26 Q. Z. Li, Q. Q. Lin, W. Z. Li, J. B. Cheng, B. A. Gong and J. Z. Sun, *ChemPhysChem*, 2008, **9**, 2265–2269.
27 M. Gao, Q. Z. Li, J. B. Cheng, W. Z. Li and H. B. Li, *RSC Adv.*, 2015, **5**, 105160–105168.
28 Q. Z. Li, R. Li, X. F. Liu, W. Z. Li and J. B. Cheng, *ChemPhysChem*, 2012, **13**, 1205–1212.
29 Q. Z. Li, H. Qi, R. Li, X. F. Liu, W. Z. Li and J. B. Cheng, *Phys. Chem. Chem. Phys.*, 2012, **14**, 3025–3030.
30 M. Gao, J. B. Cheng, X. Yang, W. Z. Li, B. Xiao and Q. Z. Li, *J. Chem. Phys.*, 2015, **143**, 054308.
31 Y. L. Zeng, W. J. Wu, X. Y. Li, S. J. Zheng and L. P. Meng, *ChemPhysChem*, 2013, **14**, 1591–1600.
32 Y. X. Lu, Y. T. Liu, H. Y. Li, X. Zhu, H. L. Liu and W. L. Zhu, *ChemPhysChem*, 2012, **13**, 2154–2161.
33 C. Estarellas, A. Frontera, D. Quiñonero and P. M. Deyà, *ChemPhysChem*, 2011, **12**, 2742–2750.
34 H. Y. Li, Y. X. Lu, Y. T. Liu, X. Zhu, H. L. Liu and W. L. Zhu, *Phys. Chem. Chem. Phys.*, 2012, **14**, 9948–9955.
35 I. Alkorta, J. Elguero, O. Mó, M. Yáñez and J. E. Del Bene, *Phys. Chem. Chem. Phys.*, 2015, **17**, 2259–2267.
36 A. Bauzá, T. J. Mooibroek and A. Frontera, *Angew. Chem., Int. Ed.*, 2013, **52**, 12317–12321.
37 R. S. Ruoff, T. Emilsson, A. I. Jaman, T. C. Germann and H. S. Gutowsky, *J. Chem. Phys.*, 1992, **96**, 3441–3446.
38 N. W. Mitzel, A. J. Blake and D. W. H. Rankin, *J. Am. Chem. Soc.*, 1997, **119**, 4143–4148.
39 I. Alkorta, I. Rozas and J. Elguero, *J. Phys. Chem. A*, 2001, **105**, 743–749.
40 M. S. Gargari, V. Stilinović, A. Bauzá, A. Frontera, P. McArdle, D. V. Derveer, S. W. Ng and G. Mahmoudi, *Chem.–Eur. J.*, 2015, **21**, 17951–17958.
41 G. Mahmoudi, A. Bauzá and A. Frontera, *Dalton Trans.*, 2016, **45**, 4965–4969.
42 A. Bauzá, A. Frontera and T. J. Mooibroek, *Phys. Chem. Chem. Phys.*, 2016, **18**, 1693–1698.
43 J. Mikosch, S. Trippel, C. Eichhorn, R. Otto, U. Lourderaj, J. X. Zhang, W. L. Hase, M. Weidemüller and R. Wester, *Science*, 2008, **319**, 183–186.
44 S. J. Grabowski, *Phys. Chem. Chem. Phys.*, 2014, **16**, 1824–1834.
45 M. X. Liu, Q. Z. Li, J. B. Cheng, W. Z. Li and H. B. Li, *J. Chem. Phys.*, 2016, **145**, 224310.
46 Q. Z. Li, X. Guo, X. Yang, W. Z. Li, J. B. Cheng and H. B. Li, *Phys. Chem. Chem. Phys.*, 2014, **16**, 11617–11625.
47 X. Guo, Y. W. Liu, Q. Z. Li, W. Z. Li and J. B. Cheng, *Chem. Phys. Lett.*, 2015, **620**, 7–12.
48 M. X. Liu, Q. Z. Li, W. Z. Li and J. B. Cheng, *J. Mol. Graphics Modell.*, 2016, **65**, 35–42.
49 M. X. Liu, L. Yang, Q. Z. Li, W. Z. Li, J. B. Cheng, B. Xiao and X. F. Yu, *J. Mol. Model.*, 2016, **22**, 192.
50 Q. J. Tang and Q. Z. Li, *Comput. Theor. Chem.*, 2014, **1050**, 51–57.
51 S. A. C. McDowell, *Chem. Phys. Lett.*, 2014, **598**, 1–4.
52 M. D. Esrafili, N. Mohammadirad and M. Solimannejad, *Chem. Phys. Lett.*, 2015, **628**, 16–20.
53 M. Solimannejad, M. Orojloo and S. Amani, *J. Mol. Model.*, 2015, **21**, 183.
54 S. Yourdkhani, T. Korona and N. L. Hadipour, *J. Comput. Chem.*, 2015, **36**, 2412–2428.
55 M. Marín-Luna, I. Alkorta and J. Elguero, *J. Phys. Chem. A*, 2016, **120**, 648–656.
56 M. D. Esrafili, R. Nurazar and F. Mohammadian-Sabet, *Mol. Phys.*, 2015, **113**, 3703–3711.
57 M. D. Esrafili and F. Mohammadian-Sabet, *Mol. Phys.*, 2016, **114**, 1528–1538.
58 M. D. Esrafili and F. Mohammadian-Sabet, *Mol. Phys.*, 2016, **114**, 83–91.
59 Z. Rezaei, M. Solimannejad and M. D. Esrafili, *Comput. Theor. Chem.*, 2015, **1074**, 101–106.
60 M. Vatanparast, E. Parvini and A. Bahadori, *Mol. Phys.*, 2016, **114**, 1478–1484.
61 W. Li, Y. Zeng, X. Li, Z. Sun and L. Meng, *Phys. Chem. Chem. Phys.*, 2016, **18**, 24672–24680.
62 M. G. Voronkov, O. M. Trofimova, E. A. Grebneva, N. F. Chernov and K. A. Abzaeva, *Russ. J. Gen. Chem.*, 2011, **81**, 2391–2411.
63 T. H. Dunning Jr, *J. Chem. Phys.*, 1989, **90**, 1007–1023.
64 R. Ahlrichs, M. Bär, M. Häcer, H. Horn and C. Komel, *Chem. Phys. Lett.*, 1989, **162**, 165–169.
65 K. A. Peterson, B. C. Shepler, D. Figgen and H. Stoll, *J. Phys. Chem. A*, 2006, **110**, 13877–13883.
66 A. Frontera, D. Quiñonero, C. Garau, P. Ballester, A. Costa and P. M. Deyà, *J. Phys. Chem. A*, 2005, **109**, 4632–4637.
67 D. Quiñonero, C. Garau, A. Frontera, P. Ballester, A. Costa and P. M. Deyà, *J. Phys. Chem. A*, 2006, **110**, 5144–5148.
68 S. B. Boys and F. Bernardy, *Mol. Phys.*, 1970, **19**, 553–566.
69 F. A. Bulat, A. Toro-Labbe, T. Brinck, J. S. Murray and P. Politzer, *J. Mol. Model.*, 2010, **16**, 1679–1691.
70 R. F. W. Bader, *AIM2000 Program, v. 2.0*, McMaster University, Hamilton, Canada, 2000.
71 A. E. Reed, L. A. Curtiss and F. Weinhold, *Chem. Rev.*, 1988, **88**, 899–926.
72 E. D. Glendening, J. K. Badenhoop, A. E. Reed, J. E. Carpenter, J. A. Bohmann, C. M. Morales and F. Weinhold, *NBO 5.0*, 2001.
73 E. R. Johnson, S. Keinan, P. Mori-Sánchez, J. Contreras-García, A. J. Cohen and W. T. Yang, *J. Am. Chem. Soc.*, 2010, **132**, 6498–6506.
74 T. Lu and F. Chen, *J. Comput. Chem.*, 2012, **3**, 580–592.
75 T. Clark, J. S. Murray and P. Politzer, *Aust. J. Chem.*, 2014, **67**, 451–456.
76 R. Rivelino and S. Canuto, *J. Phys. Chem. A*, 2001, **105**, 11260–11265.
77 W. D. Arnold and E. Oldfield, *J. Am. Chem. Soc.*, 2000, **122**, 12835–12841.

